

# Matter Effects of Sterile Neutrino in Light of Renormalization-Group Equations

---

Shuge Zeng, Fanrong Xu <sup>1</sup>

*Department of Physics and Siyuan Laboratory, Jinan University,  
Guangzhou 510632, P.R. China*

*E-mail:* [sgzeng@stu2021.jnu.edu.cn](mailto:sgzeng@stu2021.jnu.edu.cn), [fanrongxu@jnu.edu.cn](mailto:fanrongxu@jnu.edu.cn)

ABSTRACT:

The renormalization-group equation (RGE) approach to neutrino matter effects is further developed in this work. We derive a complete set of differential equations for effective mixing elements, masses and Jarlskog-like invariants in presence of a light sterile neutrino. The evolutions of mixing elements as well as Jarlskog-like invariants are obtained by numerically solving these differential equations. We calculate terrestrial matter effects in long-baseline (LBL) experiments, taking NO $\nu$ A, T2K and DUNE as examples. In both three-flavor and four-flavor frameworks, electron-neutrino survival probabilities as well as the day-night asymmetry of solar neutrino are also evaluated as a further examination of the RGE approach.

KEYWORDS: Sterile neutrino, Matter effects, Renormalization-group equations

---

<sup>1</sup>Corresponding author.

---

## Contents

<b>1</b>	<b>Introduction</b>	<b>2</b>
<b>2</b>	<b>Analytical formulae with RGE</b>	<b>4</b>
2.1	Master equations for effective masses and mixing matrix	4
2.2	The detailed differential equations	5
2.3	Effective Jarlskog-like invariants	7
2.4	General formulae for oscillation probabilities	9
<b>3</b>	<b>Applications and numerical results</b>	<b>9</b>
3.1	The evolution of mixing matrix elements	10
3.2	The evolution of Jarlskog-like invariants	12
3.3	The matter effects in Earth	13
3.4	The day-night asymmetry of solar neutrino	15
<b>4</b>	<b>Concluding remarks</b>	<b>17</b>
<b>A</b>	<b>Input parameters</b>	<b>18</b>

---

## 1 Introduction

Now it is well established that active neutrinos are massive with tiny masses and oscillate among different flavor states. The measurement of oscillation parameters are improved noticeably in the last two decades. On the other hand, as hypothetical particles, sterile neutrinos do not couple directly to the gauge bosons and can only participate in weak interactions through mixing with active neutrinos. Theoretically their mass and number are unconstrained, and have been quested in experiments for a long time. The existence of eV mass scale sterile neutrinos has been motivated by several low energy anomalies which cannot be accounted for by the standard three-flavor active neutrino framework. These involve short-baseline (SBL) experiments with neutrinos from accelerators, reactors and radioactive sources.

Two most well-known accelerator-based experiments are LSND and MiniBooNE. The LSND anomaly is the  $3.8\sigma$  excess of events compatible to  $\bar{\nu}_e$  appearance in a  $\bar{\nu}_\mu$  beam observed by the LSND experiment [1], while the MiniBooNE anomaly is the  $4.8\sigma$  excess of electron-like events in the MiniBooNE experiment observed in both  $\nu_\mu$  and  $\bar{\nu}_\mu$  beams [2]. As a direct test of LSND anomaly, the JSNS<sup>2</sup> experiment has started data taking [3] at J-PARC in Japan. With the same neutrino beam as MiniBooNE but superior event reconstruction capabilities, the MicroBooNE collaboration recently has released results scrutinizing the MiniBooNE anomaly, known as the MiniBooNE low-energy excess (MBLEE). A first MicroBooNE analysis disfavors that the MBL EE is due to underestimated production of  $\Delta$  baryons followed by decays to photons at a significance of 94.8% C.L. [4] and concluded that “no excess of  $\nu_e$  events is observed” [5]. However, a recent work shows quantitatively that the MicroBooNE collaboration “unquestionably do not probe the full parameter space of sterile neutrino models hinted at by MiniBooNE, nor do they probe the  $\nu_e$  interpretation of the MiniBooNE excess in a model-independent way” [6], which indicates that it is still early to exclude eV scale sterile neutrinos. The reactor antineutrino anomaly (RAA), is about the 6% deficit (a  $3\sigma$  effect) of  $\bar{\nu}_e$  in reactor VSBL (very short-baseline,  $< 100$  m) experiments resulting from the re-evaluation of the reactor antineutrino flux [7, 8], compared to the new prediction in 2011 [9]. Many VSBL experiments have been created and progresses have been made, including NEOS[10], DANSS[11], STEREO[12], Neutrino-4[13], PROSPECT[14] and so on. The gallium anomaly occurred in the two experiments GALLEX [15, 16] and SAGE [17, 18], where a deficit of 16% events between observations and theoretical calculation [19] was found. Though the latest estimation carried out in 2019 using new nuclear shell-model wave functions diminish the significance from  $3\sigma$  to  $2.3\sigma$  [20], recently BEST [21] reaffirmed the gallium anomaly with a larger deficit 20–24%. More can be referred to the recent review papers [22, 23].

Regardless of the sources, baselines and energy ranges of these experiments, all of the results involving above experiments can be understood individually via SBL neutrino oscillations driven by  $\Delta m^2 \sim 1\text{eV}^2$ , requiring a fourth neutrino mass eigenstate to account for this higher mass-squared difference. Hence the existence of eV mass scale light sterile neutrinos is still an open question to be answered at this stage.

The Mikheyev-Smirnov-Wolfenstein (MSW) matter effects [24, 25] plays an essential

role in the determination of neutrino mass ordering and leptonic CP-violating phase via the long-baseline (LBL) accelerator neutrino experiments. When the neutrino beam propagates in the Earth matter for a long distance, the MSW effect becomes crucially important. In presence of a light sterile neutrino, more degrees of freedom enter the MSW effect even in the propagation of active flavor neutrinos. For the calculation of matter effects involving a light sterile neutrino, different methods [26–28] have been developed in recent years.

The idea of renormalization-group equations (RGEs) has been widely applied in quantum fields theories[29, 30], solid-state physics[31, 32], and other fields of modern physics. There have been attempts to make a connection between RGE and neutrino matter effects in the past few years[33, 34]. Recently, more progress has been made [35–37]. By taking the matter term  $a$  (see Section 2) as the role of renormalization energy scale, a close set of differential equations describing the evolution of effective mixing matrix and effective mass-square differences in three-flavor case has been established [35]. The analytical solutions for the mixing and masses are further given in [37]. One may naturally wonder whether it is accessible to extend the RGE framework to include the sterile neutrino contribution. In addition to developing the form theoretically, it is also interesting to realize the practical application of this new method in neutrino phenomenology. These topics are supposed to be investigated in current work. Although it does not participate weak interactions directly, the sterile neutrino contribution in Hamiltonian is brought in through subtracting a global identical term produced via charged lepton neutral-current, denoted as mass term  $a'$  (see Section 2). In the scenario of constant density matter, two mass terms of electron-type and sterile neutrino is connected by a constant  $k$ . Then we can continue working in the framework of RGE approach [35], and extend the evolution of mixing matrix and mass-square differences with respect to mass term  $a$  (or equivalently neutrino beam energy  $E$ ), including the sterile neutrino contribution. After analytically deriving the completed set of differential equations, we further explore their solutions numerically. In principle, oscillation probabilities should be calculable in the RGE approach, which now is realized here for the first time in both cases with purely three active neutrinos as well as with one more sterile neutrino. We take three LBL accelerator neutrino experiments, NOvA, T2K and DUNE, as typical examples to test the validity of RGE approach in practical numerical analysis and find that the results perfectly agree with the analytical approach [27]. In the adiabatic approximation of solar matter and slab approximation of Earth matter, we also calculate the day-night asymmetry observed in the surface of Earth, as a further application of RGE method.

The remaining part of this paper is organized as follows. In Section 2, we present the derivation details and exact forms of differential equations of masses and mixing matrix, as well as oscillation probabilities. After exhibiting the explicit evolution of mixing matrix elements involving a light sterile neutrino in first part of Section 3, we further apply the methodology to Earth matter effects in three LBL experiments and solar matter effects in name of day-night asymmetry. We conclude the validity of RGE approach in Section 4 and related input parameters are summarized in Appendix A.

## 2 Analytical formulae with RGE

It is known that physical observables are independent of energy scale while parameters describing the observables depend on scale themselves, and renormalization-group equations (RGEs) depict the evolutions of these parameters with respect to the energy scale. With the general idea of RGE, a new method is developed to describe flavor mixing parameters evolve when neutrinos propagate in a medium in the framework of three-flavor neutrino oscillation[35]. As introduced in Sec.1, the existence of eV-scale light sterile neutrinos is still an open question and the calculation of matter effects with sterile neutrino is meaningful, especially in the measurement of mass ordering and leptonic CP-violating phase(es). In this section, we will make an extension of the RGE approach to contain the case in presence of a light sterile neutrino in addition to three active flavors.

### 2.1 Master equations for effective masses and mixing matrix

Similar to the standard three-flavor case, the effective Hamiltonian with sterile neutrino contribution is given as

$$H_m = \frac{1}{2E} \left[ U \begin{pmatrix} m_1^2 & 0 & 0 & 0 \\ 0 & m_2^2 & 0 & 0 \\ 0 & 0 & m_3^2 & 0 \\ 0 & 0 & 0 & m_4^2 \end{pmatrix} U^\dagger + \begin{pmatrix} a & 0 & 0 & 0 \\ 0 & 0 & 0 & 0 \\ 0 & 0 & 0 & 0 \\ 0 & 0 & 0 & a' \end{pmatrix} \right] \equiv \frac{1}{2E} V \begin{pmatrix} \tilde{m}_1^2 & 0 & 0 & 0 \\ 0 & \tilde{m}_2^2 & 0 & 0 \\ 0 & 0 & \tilde{m}_3^2 & 0 \\ 0 & 0 & 0 & \tilde{m}_4^2 \end{pmatrix} V^\dagger, \quad (2.1)$$

where  $a \equiv 2\sqrt{2}G_F N_e E$  with  $N_e$  being the net electron number density and  $E$  the neutrino beam energy, mass terms  $m_i^2$  and  $\tilde{m}_i^2$  in vacuum and matter, respectively. For the mixing matrices, the mixing in vacuum (PMNS matrix) is denoted as  $U$ <sup>1</sup> and  $V$  stands for the effective mixing incorporating matter effects. Though it does not take part in weak interaction itself, the sterile neutrino has an matter effects term  $a'$  here due to the subtraction of a global identical term produced via neutral-current interaction of active neutrinos. In general,  $a'$  depends on the medium neutrino beam propagating. In the scenario of constant density matter, we can further write down  $a' = ka$  and the medium information is encoded in the matter parameter  $k$ .

We take  $a$  as the role of energy scale in RGE similar as [35]. Differentiating both sides of Eq.(2.1) with respect to  $a$ , we have

$$\begin{aligned} \dot{D} + [V^\dagger \dot{V}, D] &= V^\dagger \begin{pmatrix} 1 & 0 & 0 & 0 \\ 0 & 0 & 0 & 0 \\ 0 & 0 & 0 & 0 \\ 0 & 0 & 0 & k \end{pmatrix} V \\ &= \begin{pmatrix} |V_{e1}|^2 + k|V_{s1}|^2 & V_{e1}^* V_{e2} + kV_{s1}^* V_{s2} & V_{e1}^* V_{e3} + kV_{s1}^* V_{s3} & V_{e1}^* V_{e4} + kV_{s1}^* V_{s4} \\ V_{e2}^* V_{e1} + kV_{s2}^* V_{s1} & |V_{e2}|^2 + k|V_{s2}|^2 & V_{e2}^* V_{e3} + kV_{s2}^* V_{s3} & V_{e2}^* V_{e4} + kV_{s2}^* V_{s4} \\ V_{e3}^* V_{e1} + kV_{s3}^* V_{s1} & V_{e3}^* V_{e2} + kV_{s3}^* V_{s2} & |V_{e3}|^2 + k|V_{s3}|^2 & V_{e3}^* V_{e4} + kV_{s3}^* V_{s4} \\ V_{e4}^* V_{e1} + kV_{s4}^* V_{s1} & V_{e4}^* V_{e2} + kV_{s4}^* V_{s2} & V_{e4}^* V_{e3} + kV_{s4}^* V_{s3} & |V_{e4}|^2 + k|V_{s4}|^2 \end{pmatrix}, \end{aligned} \quad (2.2)$$

where  $D \equiv \text{diag} \{ \tilde{m}_1^2, \tilde{m}_2^2, \tilde{m}_3^2, \tilde{m}_4^2 \}$ . Apparently, the first term in the left-handed side of Eq. (2.2) is diagonal while diagonal entries of the second term vanish. Extracting the

<sup>1</sup>The convention and inputs to parameterize PMNS matrix  $U$  is introduced in Appendix A.

diagonal entries in both sides, we can firstly get a relation

$$\frac{d\tilde{m}_i^2}{da} = |V_{ei}|^2 + k|V_{si}|^2,$$

which further leads to the first order differential equations

$$\frac{d}{da}\Delta\tilde{m}_{ij}^2 = (|V_{ei}|^2 - |V_{ej}|^2) + k(|V_{si}|^2 - |V_{sj}|^2) \quad (2.3)$$

with the effective mass square difference  $\Delta\tilde{m}_{ij}^2 \equiv \tilde{m}_i^2 - \tilde{m}_j^2$ . Similarly, by comparing the off-diagonal entries in Eq. (2.2), one has

$$\sum_{\alpha} V_{\alpha i}^* \dot{V}_{\alpha j} = (\Delta\tilde{m}_{ji}^2)^{-1} (V_{ei}^* V_{ej} + kV_{si}^* V_{sj}). \quad (2.4)$$

Multiply both sides of the orthogonal relation

$$\sum_{j \neq i} V_{\alpha j}^* V_{\beta j} = \delta_{\alpha\beta} - V_{\alpha i}^* V_{\beta i},$$

with  $\dot{V}_{\alpha i}$ , and take a summation over  $\alpha$  (so that  $\sum_{\alpha} \dot{V}_{\alpha i} V_{\alpha i}^* = 0$ ), we can write down the differential equation for effective mixing matrix as

$$\dot{V}_{\beta i} = \sum_{j \neq i} V_{\beta j} (V_{ej}^* V_{ei} + kV_{sj}^* V_{si}) (\Delta\tilde{m}_{ij}^2)^{-1}, \quad (2.5)$$

in which Eq. (2.4) is applied and summation is not taken for index  $i$ . Due to the fact

$$\sum_{\beta} \dot{V}_{\beta i}^* V_{\beta i} V_{\alpha i}^* V_{\alpha i} + \sum_{\beta} V_{\alpha i}^* V_{\alpha i} \dot{V}_{\beta i} V_{\beta i}^* = |V_{\alpha i}|^2 \sum_{\beta} (\dot{V}_{\beta i}^* V_{\beta i} + \dot{V}_{\beta i} V_{\beta i}^*) = 0,$$

the differential equation of mixing matrix can also be written in terms of the square of mixing matrix,

$$\frac{d}{da}|V_{\alpha i}|^2 = \left( \frac{d}{da} V_{\alpha i}^* \right) V_{\alpha i} + V_{\alpha i}^* \frac{d}{da} V_{\alpha i} = 2 \sum_{j \neq i} \text{Re} [V_{\alpha j} V_{\alpha i}^* (V_{ej}^* V_{ei} + kV_{sj}^* V_{si})] (\Delta\tilde{m}_{ij}^2)^{-1}, \quad (2.6)$$

this compact form is phase-independent and brings convenience in some parts of following calculation.

## 2.2 The detailed differential equations

The master equations (2.3) and (2.6) (or (2.5)) form a closed and complete equation group, which contains 19 independent differential equations. To have a global impression, it is helpful to exhibit some necessary differential equations explicitly. Three independent equations on mass square differences can be detailed from equation (2.3),

$$\begin{aligned} \frac{d}{da}\Delta\tilde{m}_{12}^2 &= (|V_{e1}|^2 - |V_{e2}|^2) + k(|V_{s1}|^2 - |V_{s2}|^2), \\ \frac{d}{da}\Delta\tilde{m}_{13}^2 &= (|V_{e1}|^2 - |V_{e3}|^2) + k(|V_{s1}|^2 - |V_{s3}|^2), \\ \frac{d}{da}\Delta\tilde{m}_{14}^2 &= (|V_{e1}|^2 - |V_{e4}|^2) + k(|V_{s1}|^2 - |V_{s4}|^2). \end{aligned} \quad (2.7)$$

The right handed side of equation (2.7) indicates that the evolution property of mass square difference relies on square of mixing matrix entries together with the matter parameter  $k$ . As part of the closed equation group, the detailed differential equations for  $\alpha = e$  can be read from equation (2.6),

$$\begin{aligned}
\frac{d}{da}|V_{e1}|^2 &= 2|V_{e1}|^2 [ |V_{e2}|^2(\Delta\tilde{m}_{12}^2)^{-1} - |V_{e3}|^2(\Delta\tilde{m}_{31}^2)^{-1} - |V_{e4}|^2(\Delta\tilde{m}_{41}^2)^{-1} ] \\
&\quad + 2k\text{Re} \left[ V_{e1}^* V_{s1} \left( V_{e2} V_{s2}^* (\Delta\tilde{m}_{12}^2)^{-1} - V_{e3} V_{s3}^* (\Delta\tilde{m}_{31}^2)^{-1} - V_{e4} V_{s4}^* (\Delta\tilde{m}_{41}^2)^{-1} \right) \right], \\
\frac{d}{da}|V_{e2}|^2 &= 2|V_{e2}|^2 [ |V_{e3}|^2(\Delta\tilde{m}_{23}^2)^{-1} - |V_{e4}|^2(\Delta\tilde{m}_{42}^2)^{-1} - |V_{e1}|^2(\Delta\tilde{m}_{12}^2)^{-1} ] \\
&\quad + 2k\text{Re} \left[ V_{e2}^* V_{s2} \left( V_{e1} V_{s1}^* (\Delta\tilde{m}_{21}^2)^{-1} - V_{e3} V_{s3}^* (\Delta\tilde{m}_{32}^2)^{-1} - V_{e4} V_{s4}^* (\Delta\tilde{m}_{42}^2)^{-1} \right) \right], \\
\frac{d}{da}|V_{e3}|^2 &= 2|V_{e3}|^2 [ |V_{e4}|^2(\Delta\tilde{m}_{34}^2)^{-1} - |V_{e1}|^2(\Delta\tilde{m}_{13}^2)^{-1} - |V_{e2}|^2(\Delta\tilde{m}_{23}^2)^{-1} ] \\
&\quad + 2k\text{Re} \left[ V_{e3}^* V_{s3} \left( V_{e4} V_{s4}^* (\Delta\tilde{m}_{34}^2)^{-1} - V_{e1} V_{s1}^* (\Delta\tilde{m}_{13}^2)^{-1} - V_{e2} V_{s2}^* (\Delta\tilde{m}_{23}^2)^{-1} \right) \right], \\
\frac{d}{da}|V_{e4}|^2 &= 2|V_{e4}|^2 [ |V_{e1}|^2(\Delta\tilde{m}_{41}^2)^{-1} - |V_{e2}|^2(\Delta\tilde{m}_{24}^2)^{-1} - |V_{e3}|^2(\Delta\tilde{m}_{34}^2)^{-1} ] \\
&\quad + 2k\text{Re} \left[ V_{e4}^* V_{s4} \left( V_{e1} V_{s1}^* (\Delta\tilde{m}_{41}^2)^{-1} - V_{e2} V_{s2}^* (\Delta\tilde{m}_{24}^2)^{-1} - V_{e3} V_{s3}^* (\Delta\tilde{m}_{34}^2)^{-1} \right) \right].
\end{aligned} \tag{2.8}$$

The evolution equations of  $|V_{\alpha i}|^2$ , taking  $|V_{ei}|^2$  as an example, contain more information than the ones of  $\Delta\tilde{m}_{ij}^2$  for their entanglement with mass-square differences, as well as individual mixing matrix elements. From the known the general expression for the evolution of  $V_{\alpha i}$  with respect to  $a$  equation (2.5), we can further write down explicitly those related to electron-type neutrino and sterile neutrino, giving

$$\begin{aligned}
\frac{dV_{e1}}{da} &= (V_{e1}|V_{e2}|^2 + kV_{e2}V_{s1}V_{s2}^*)(\Delta\tilde{m}_{12}^2)^{-1} - (V_{e1}|V_{e3}|^2 + kV_{e3}V_{s1}V_{s3}^*)(\Delta\tilde{m}_{31}^2)^{-1} \\
&\quad - (V_{e1}|V_{e4}|^2 + kV_{e4}V_{s1}V_{s4}^*)(\Delta\tilde{m}_{41}^2)^{-1}, \\
\frac{dV_{e2}}{da} &= (V_{e2}|V_{e1}|^2 + kV_{e1}V_{s2}V_{s1}^*)(\Delta\tilde{m}_{21}^2)^{-1} - (V_{e2}|V_{e3}|^2 + kV_{e3}V_{s2}V_{s3}^*)(\Delta\tilde{m}_{32}^2)^{-1} \\
&\quad - (V_{e2}|V_{e4}|^2 + kV_{e4}V_{s2}V_{s4}^*)(\Delta\tilde{m}_{42}^2)^{-1}, \\
\frac{dV_{e3}}{da} &= (V_{e3}|V_{e1}|^2 + kV_{e1}V_{s3}V_{s1}^*)(\Delta\tilde{m}_{31}^2)^{-1} - (V_{e3}|V_{e2}|^2 + kV_{e2}V_{s3}V_{s2}^*)(\Delta\tilde{m}_{23}^2)^{-1} \\
&\quad - (V_{e3}|V_{e4}|^2 + kV_{e4}V_{s3}V_{s4}^*)(\Delta\tilde{m}_{43}^2)^{-1}, \\
\frac{dV_{e4}}{da} &= (V_{e4}|V_{e1}|^2 + kV_{e1}V_{s4}V_{s1}^*)(\Delta\tilde{m}_{41}^2)^{-1} + (V_{e4}|V_{e2}|^2 + kV_{e2}V_{s4}V_{s2}^*)(\Delta\tilde{m}_{42}^2)^{-1} \\
&\quad + (V_{e4}|V_{e3}|^2 + kV_{e3}V_{s4}V_{s3}^*)(\Delta\tilde{m}_{43}^2)^{-1},
\end{aligned} \tag{2.9}$$

and

$$\begin{aligned}
\frac{dV_{s1}}{da} &= (V_{s2}V_{e2}^*V_{e1} + k|V_{s2}|^2V_{s1})(\Delta\tilde{m}_{12}^2)^{-1} - (V_{s3}V_{e3}^*V_{e1} + k|V_{s3}|^2V_{s1})(\Delta\tilde{m}_{31}^2)^{-1} \\
&\quad - (V_{s4}V_{e4}^*V_{e1} + k|V_{s4}|^2V_{s1})(\Delta\tilde{m}_{41}^2)^{-1}, \\
\frac{dV_{s2}}{da} &= (V_{s1}V_{e1}^*V_{e2} + k|V_{s1}|^2V_{s2})(\Delta\tilde{m}_{21}^2)^{-1} - (V_{s3}V_{e3}^*V_{e2} + k|V_{s3}|^2V_{s2})(\Delta\tilde{m}_{32}^2)^{-1} \\
&\quad - (V_{s4}V_{e4}^*V_{e2} + k|V_{s4}|^2V_{s2})(\Delta\tilde{m}_{42}^2)^{-1}, \\
\frac{dV_{s3}}{da} &= (V_{s1}V_{e1}^*V_{e3} + k|V_{s1}|^2V_{s3})(\Delta\tilde{m}_{31}^2)^{-1} - (V_{s2}V_{e2}^*V_{e3} + k|V_{s2}|^2V_{s3})(\Delta\tilde{m}_{23}^2)^{-1} \\
&\quad - (V_{s4}V_{e4}^*V_{e3} + k|V_{s4}|^2V_{s3})(\Delta\tilde{m}_{43}^2)^{-1}, \\
\frac{dV_{s4}}{da} &= (V_{s1}V_{e1}^*V_{e4} + k|V_{s1}|^2V_{s4})(\Delta\tilde{m}_{41}^2)^{-1} + (V_{s2}V_{e2}^*V_{e4} + k|V_{s2}|^2V_{s4})(\Delta\tilde{m}_{42}^2)^{-1} \\
&\quad - (V_{s3}V_{e3}^*V_{e4} + k|V_{s3}|^2V_{s4})(\Delta\tilde{m}_{43}^2)^{-1}.
\end{aligned} \tag{2.10}$$

Although equations (2.9) and (2.8) are not independent ones, here for the purpose of solving the tangled differential equations a clear exhibition is useful and helpful. Combining above equations together, the masses and mixings involving electron-type and sterile neutrino are in principle calculable, which further provide input to solve the mixings involving muon and tau neutrinos,

$$\begin{aligned}
\frac{d}{da}|V_{\mu 1}|^2 &= 2\text{Re} \left[ V_{\mu 1}^* V_{e 1} \left( V_{\mu 2} V_{e 2}^* (\Delta\tilde{m}_{12}^2)^{-1} - V_{\mu 3} V_{e 3}^* (\Delta\tilde{m}_{31}^2)^{-1} - V_{\mu 4} V_{e 4}^* (\Delta\tilde{m}_{41}^2)^{-1} \right) \right] \\
&\quad + 2k\text{Re} \left[ V_{\mu 1}^* V_{s 1} \left( V_{\mu 2} V_{s 2}^* (\Delta\tilde{m}_{12}^2)^{-1} - V_{\mu 3} V_{s 3}^* (\Delta\tilde{m}_{31}^2)^{-1} - V_{\mu 4} V_{s 4}^* (\Delta\tilde{m}_{41}^2)^{-1} \right) \right], \\
\frac{d}{da}|V_{\mu 2}|^2 &= 2\text{Re} \left[ V_{\mu 2}^* V_{e 2} \left( V_{\mu 1} V_{e 1}^* (\Delta\tilde{m}_{21}^2)^{-1} - V_{\mu 3} V_{e 3}^* (\Delta\tilde{m}_{32}^2)^{-1} - V_{\mu 4} V_{e 4}^* (\Delta\tilde{m}_{42}^2)^{-1} \right) \right] \\
&\quad + 2k\text{Re} \left[ V_{\mu 2}^* V_{s 2} \left( V_{\mu 1} V_{s 1}^* (\Delta\tilde{m}_{21}^2)^{-1} - V_{\mu 3} V_{s 3}^* (\Delta\tilde{m}_{32}^2)^{-1} - V_{\mu 4} V_{s 4}^* (\Delta\tilde{m}_{42}^2)^{-1} \right) \right], \\
\frac{d}{da}|V_{\mu 3}|^2 &= 2\text{Re} \left[ V_{\mu 3}^* V_{e 3} \left( V_{\mu 2} V_{e 2}^* (\Delta\tilde{m}_{32}^2)^{-1} + V_{\mu 1} V_{e 1}^* (\Delta\tilde{m}_{31}^2)^{-1} - V_{\mu 4} V_{e 4}^* (\Delta\tilde{m}_{43}^2)^{-1} \right) \right] \\
&\quad + 2k\text{Re} \left[ V_{\mu 3}^* V_{s 3} \left( V_{\mu 2} V_{s 2}^* (\Delta\tilde{m}_{32}^2)^{-1} + V_{\mu 1} V_{s 1}^* (\Delta\tilde{m}_{31}^2)^{-1} - V_{\mu 4} V_{s 4}^* (\Delta\tilde{m}_{43}^2)^{-1} \right) \right], \\
\frac{d}{da}|V_{\mu 4}|^2 &= 2\text{Re} \left[ V_{\mu 4}^* V_{e 4} \left( V_{\mu 2} V_{e 2}^* (\Delta\tilde{m}_{42}^2)^{-1} + V_{\mu 3} V_{e 3}^* (\Delta\tilde{m}_{43}^2)^{-1} + V_{\mu 1} V_{e 1}^* (\Delta\tilde{m}_{41}^2)^{-1} \right) \right] \\
&\quad + 2k\text{Re} \left[ V_{\mu 4}^* V_{s 4} \left( V_{\mu 2} V_{s 2}^* (\Delta\tilde{m}_{42}^2)^{-1} + V_{\mu 3} V_{s 3}^* (\Delta\tilde{m}_{43}^2)^{-1} + V_{\mu 1} V_{s 1}^* (\Delta\tilde{m}_{41}^2)^{-1} \right) \right].
\end{aligned} \tag{2.11}$$

The differential equations on tau flavor has been neglected here as they take the similar form as muon. Among all the equations in the whole equation group, equations (2.7) and (2.8) play a key role to solve all the equations. The sterile neutrino contributions are characterized both by matter parameter  $k$  and the mixings involving the fourth row and column. By vanishing the sterile neutrino related mixing matrix elements,  $V_{\alpha 4} (\alpha = e, \dots, s)$  and  $V_{s i} (i = 1, \dots, 4)$ , equations (2.7) and (2.8) return to standard three-flavor case [35].

### 2.3 Effective Jarlskog-like invariants

The Jarlskog invariant [38], defined as the imaginary part of products of mixing matrix elements, is an important measurement to characterize the CP violation in fermion sector.



It is known that there is only one independent invariant in models with fermion family number being three. Previously there have been some discussions on Jarlskog-like invariants beyond three generation of quarks [39] and leptons [40]. Here in this work by incorporating a light sterile neutrino, we define the effective Jarlskog-like invariants

$$\mathcal{J}_{\alpha\beta}^{ij} = \text{Im}(U_{\alpha i}U_{\beta j}U_{\alpha j}^*U_{\beta i}^*), \quad \tilde{\mathcal{J}}_{\alpha\beta}^{ij} = \text{Im}(V_{\alpha i}V_{\beta j}V_{\alpha j}^*V_{\beta i}^*) \quad (2.12)$$

in vacuum as  $\mathcal{J}$  and its counterpart  $\tilde{\mathcal{J}}$  in matter, in which  $\alpha, \beta = e, \mu, \tau, s$  and  $i, j = 1, 2, 3, 4$ . From the fact  $\mathcal{J}_{\alpha\alpha}^{ij} = \mathcal{J}_{\alpha\beta}^{ii} = 0$  and

$$\sum_i \mathcal{J}_{\alpha\beta}^{ij} = \sum_j \mathcal{J}_{\alpha\beta}^{ij} = \sum_\alpha \mathcal{J}_{\alpha\beta}^{ij} = \sum_\beta \mathcal{J}_{\alpha\beta}^{ij} = 0 \quad (2.13)$$

due to the unitary condition of the mixing matrix, the number of independent Jarlskog-like invariants increases to 9 compared with 1 in the three-flavor case, which holds for the counterpart in matter.

The differential equation for the Jarlskog-like invariants can be derived by using equation (2.5) after a straightforward algebraic calculation,

$$\begin{aligned} \frac{d}{da} \tilde{\mathcal{J}}_{\alpha\beta}^{ij} &= \sum_{k \neq i} \text{Im} [V_{\alpha j}^* V_{\beta i}^* V_{\alpha k} V_{\beta j} (V_{ek}^* V_{ei} + k V_{sk}^* V_{si})] (\Delta \tilde{m}_{ik}^2)^{-1} \\ &+ \sum_{k \neq i} \text{Im} [V_{\alpha i} V_{\beta j} V_{\alpha j}^* V_{\beta k}^* (V_{ek} V_{ei}^* + k V_{sk} V_{si}^*)] (\Delta \tilde{m}_{ik}^2)^{-1} + (\alpha \leftrightarrow \beta, i \leftrightarrow j). \end{aligned} \quad (2.14)$$

As an example, we take  $(\alpha\beta, ij) = (e\mu, 12)$  and show explicitly the evolution equation of one of the Jarlskog-like invariants in matter,

$$\begin{aligned} \frac{d}{da} \tilde{\mathcal{J}}_{e\mu}^{12} &= \tilde{\mathcal{J}}_{e\mu}^{12} \left( \frac{|V_{e2}|^2}{\Delta \tilde{m}_{12}^2} + \frac{|V_{e3}|^2}{\Delta \tilde{m}_{13}^2} + \frac{|V_{e4}|^2}{\Delta \tilde{m}_{14}^2} \right) + \frac{|V_{e1}|^2}{\Delta \tilde{m}_{13}^2} \tilde{\mathcal{J}}_{e\mu}^{32} + \frac{|V_{e1}|^2}{\Delta \tilde{m}_{14}^2} \tilde{\mathcal{J}}_{e\mu}^{42} \\ &+ \tilde{\mathcal{J}}_{e\mu}^{12} \left( \frac{|V_{e1}|^2}{\Delta \tilde{m}_{21}^2} + \frac{|V_{e3}|^2}{\Delta \tilde{m}_{23}^2} + \frac{|V_{e4}|^2}{\Delta \tilde{m}_{24}^2} \right) + \frac{|V_{e2}|^2}{\Delta \tilde{m}_{23}^2} \tilde{\mathcal{J}}_{e\mu}^{13} + \frac{|V_{e2}|^2}{\Delta \tilde{m}_{24}^2} \tilde{\mathcal{J}}_{e\mu}^{14} \\ &+ k \left( \frac{|V_{e2}|^2 \tilde{\mathcal{J}}_{\mu s}^{21}}{\Delta \tilde{m}_{12}^2} + \frac{\text{Im} [V_{\mu 2} V_{e2}^* V_{\mu 1} V_{e3} V_{s1} V_{s3}^*]}{\Delta \tilde{m}_{13}^2} + \frac{\text{Im} [V_{\mu 2} V_{e2}^* V_{\mu 1} V_{e4} V_{s1} V_{s4}^*]}{\Delta \tilde{m}_{14}^2} \right) \\ &+ k \left( \frac{|V_{\mu 2}|^2 \tilde{\mathcal{J}}_{es}^{12}}{\Delta \tilde{m}_{12}^2} + \frac{\text{Im} [V_{e1} V_{\mu 2} V_{e2}^* V_{\mu 3} V_{s3} V_{s1}^*]}{\Delta \tilde{m}_{13}^2} + \frac{\text{Im} [V_{e1} V_{\mu 2} V_{e2}^* V_{\mu 4} V_{s4} V_{s1}^*]}{\Delta \tilde{m}_{14}^2} \right) \\ &+ k \left( \frac{|V_{e1}|^2 \tilde{\mathcal{J}}_{\mu s}^{21}}{\Delta \tilde{m}_{21}^2} + \frac{\text{Im} [V_{e1} V_{\mu 2} V_{\mu 1}^* V_{e3}^* V_{s3} V_{s2}^*]}{\Delta \tilde{m}_{23}^2} + \frac{\text{Im} [V_{e1} V_{\mu 2} V_{\mu 1}^* V_{e4}^* V_{s4} V_{s2}^*]}{\Delta \tilde{m}_{24}^2} \right) \\ &+ k \left( \frac{|V_{\mu 1}|^2 \tilde{\mathcal{J}}_{es}^{12}}{\Delta \tilde{m}_{21}^2} + \frac{\text{Im} [V_{e1} V_{e2}^* V_{\mu 1}^* V_{\mu 3} V_{s2} V_{s3}^*]}{\Delta \tilde{m}_{23}^2} + \frac{\text{Im} [V_{e1} V_{e2}^* V_{\mu 1}^* V_{\mu 4} V_{s2} V_{s4}^*]}{\Delta \tilde{m}_{24}^2} \right), \end{aligned} \quad (2.15)$$

which recovers the standard three-active-flavor case in the limit of  $\tilde{m}_4 \rightarrow \infty$  and  $k \rightarrow 0$ . More Jarlskog-like invariants enter equation (2.15) compared with the general form,

equation (2.14), since the special roles of electron and sterile neutrino play. In the following numerical analysis, we will present evolutions of all the 9 Jarlskog-like invariants completely.

In addition, it can be verified that the relation

$$\sum_{i=1}^4 \frac{d}{da} \ln |V_{ei}|^2 + 2 \sum_{j>k} \frac{d}{da} \ln \Delta \tilde{m}_{jk}^2 = 0 \quad (2.16)$$

holds in the limit of  $k = 0$ , corresponding to equation (16) of [35]. On the other hand, the Naumov-like [41] and Toshev-like [42] relation in RGE approach will be explored in a separate work [43] due to its complication.

## 2.4 General formulae for oscillation probabilities

The mixing matrix and mass square differences calculated above are not physical observables themselves. In fact, they are encoded in neutrino oscillations. By replacing the mixing and mass in the vacuum with corresponding ones in matter, the general form of neutrino oscillation probability can be obtain

$$P(\nu_\alpha \rightarrow \nu_\beta) = \sum_i |V_{\alpha i}|^2 |V_{\beta i}|^2 + 2 \sum_{i<j} \left[ \text{Re}(V_{\alpha i} V_{\beta j} V_{\alpha j}^* V_{\beta i}^*) \cos \tilde{\Delta}_{ij} - \text{Im}(V_{\alpha i} V_{\beta j} V_{\alpha j}^* V_{\beta i}^*) \sin \tilde{\Delta}_{ij} \right] \quad (2.17)$$

with  $\tilde{\Delta}_{ij} \equiv \frac{\Delta \tilde{m}_{ij}^2 L}{2E}$ . We will see equation (2.17) is the most generic expression to incorporate all situations of the neutrino oscillation supported by the following facts:

- Making use of the replacement rule  $V_{ij} \leftrightarrow V_{ij}^*$ , the oscillations among antineutrinos can also be calculated by equation (2.17).
- Apparently oscillations occurring in both vacuum and matter are applicable, which depends on the choice of mixing and mass parameters,  $(U, m_i)$  or  $(V, \tilde{m}_i)$ .
- It can be utilized to describe oscillations among both in three pure active flavor case and three active together with one sterile case. The former one can be easily trended to by vanishing  $V_{si}$  ( $i = 1, \dots, 4$ ) and  $V_{\alpha 4}$  ( $\alpha = e, \dots, s$ ).

So far analytical tools for further exploring neutrino phenomenology have been prepared. We will examine this method in practical numerical study in the following part.

## 3 Applications and numerical results

To establish the connection between RGE and neutrino matter effects is more than a concept formally. In practical qualitative analysis, the RGE approach is also valuable and we will realize it here. In this section, we first numerically analyze the evolution of effective mixing matrix explicitly. Then we utilize the general oscillation eq. (2.17) together with RGE approach to effective mixing and mass in Earth and solar matters to calculate corresponding observables and the numerical results are presented, respectively.

### 3.1 The evolution of mixing matrix elements

The propagation of neutrino in various mediums depends on effective mixing matrix in different materials, hence it is necessary to perform an explicit analysis of detailed mixing matrix elements firstly. In constant density matters, the features of matter effects are controlled by the matter parameter  $k$ . For example, it is known that  $k = -0.5$  depicts earth matter. By adopting the input parameters in Appendix A, we show in Fig.1 the evolution of effective mixing matrix elements with particular  $k$  in normal hierarchy (NH) case with respect to energy scale  $a/\Delta m_{21}^2$ , where neutrinos and antineutrinos are characterized as solid red and dashed blue curves, respectively.

The situation for  $k = 0$  is special. For an illustration, we take the first row of Fig.1(a) as an example to interpret the evolutions of  $|V_{\alpha i}|^2$  according to equation (2.8). The negative (positive) sign of the right hand side of  $|V_{e1}|^2$  ( $|V_{e4}|^2$ ) evolution equation indicates a monotonic increasing (decreasing) behavior for  $|V_{e1}|^2$  ( $|V_{e4}|^2$ ). Due to a competition between positive and negative parts in the RGE equations, combining their particular initial values, the maximums appear for the evolution of  $|V_{e2}|^2$  and  $|V_{e3}|^2$ . In the large  $\Delta\tilde{m}_{41}^2$  limit, the sterile neutrino contribution is decoupled and the evolutions return to three pure active flavor case.<sup>2</sup> Comparing the left three columns of the rows except the last one (the mixings among three active flavors) in Fig.1(a) with the plot Fig.1 of [35], one can observe the behaviors of evolution curves are consistent with each other. Both the evolution behaviors and initial values of  $|V_{\mu i}|^2$ , standing for vacuum matrix elements  $|U_{\mu i}|^2$ , are qualitatively identical to  $|V_{\tau i}|^2$  ( $i = 1, 2, 3$ ). The approximate  $\mu - \tau$  symmetry is kept and well understood as the flavors are indistinguishable for muon and tau for the universal neutral-current interactions of the two flavors in ordinary matter. Mathematically, this can also be explained by setting zero values to  $k$  and  $(\Delta\tilde{m}_{41}^2)^{-1}$  in the first three equations of (2.8) and (2.11). Among all the six active-sterile mixing matrix elements for neutrino case (red solid curves), only two of them  $|V_{e4}|^2$  and  $|V_{s3}|^2$  manifest themselves as unity when energy scale  $a$  reaches around  $m_4^2$  (or  $a/\Delta m_{21}^2 \sim \Delta m_{41}^2/\Delta m_{21}^2 \sim 1000$ ). In contrast, there is no mixing among active and sterile flavors for antineutrinos. For the pure sterile neutrino,  $|V_{s4}|^2$  keeps unity and drops to small value near to zero when  $a$  approaches  $\Delta m_{41}^2 \sim 10^3 \Delta m_{21}^2$ , which guarantees the unitary conditions  $\sum_{i=1}^4 |V_{\alpha i}|^2 = 1$  for a particular flavor  $\alpha$  and  $\sum_{\alpha=e}^s |V_{\alpha i}|^2 = 1$  for a particular mass index  $i$ .

The case of  $k = -0.5$ , corresponding to the terrestrial matter, contains the contribution from non-vanishing  $k$  terms, which reflects complete sterile neutrino contributions in constant density matter. In addition to the well respected unitary conditions, some obvious changes occur in Fig.1(b):

- The effective  $\mu - \tau$  symmetry is partially breaking for  $i = 1, 2, 3$  in neutrino case and  $i = 3, 4$  for antineutrino case.

---

<sup>2</sup>The standard three-flavor limit can also be obtained by setting  $V_{\alpha 4} = 0$  and  $V_{s i} = 0$  as aforementioned. Here we understand  $3\nu$  picture in this way is for the purpose of examining corresponding results in [35].

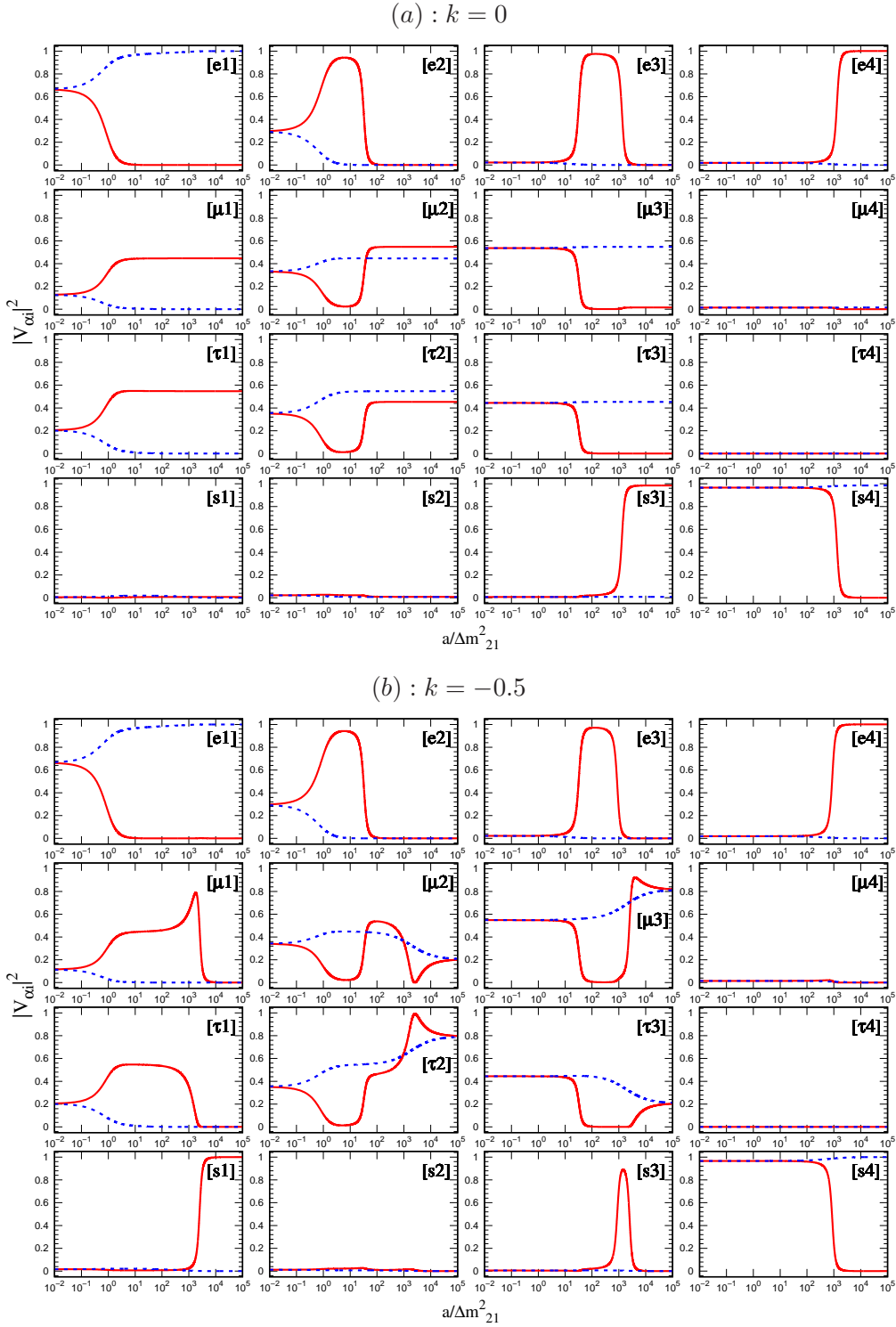


**Figure 1.** The evolution of  $|V_{\alpha i}|^2$  (for  $\alpha = e, \mu, \tau, s$  and  $i = 1, 2, 3, 4$ ) in NH case with respect to energy scale  $a/\Delta m_{21}^2$ , in which:  $k = 0$  in (a) and  $k = -0.5$  in (b). The red solid and blue dashed curves correspond to the results of neutrino and antineutrino oscillations, respectively.

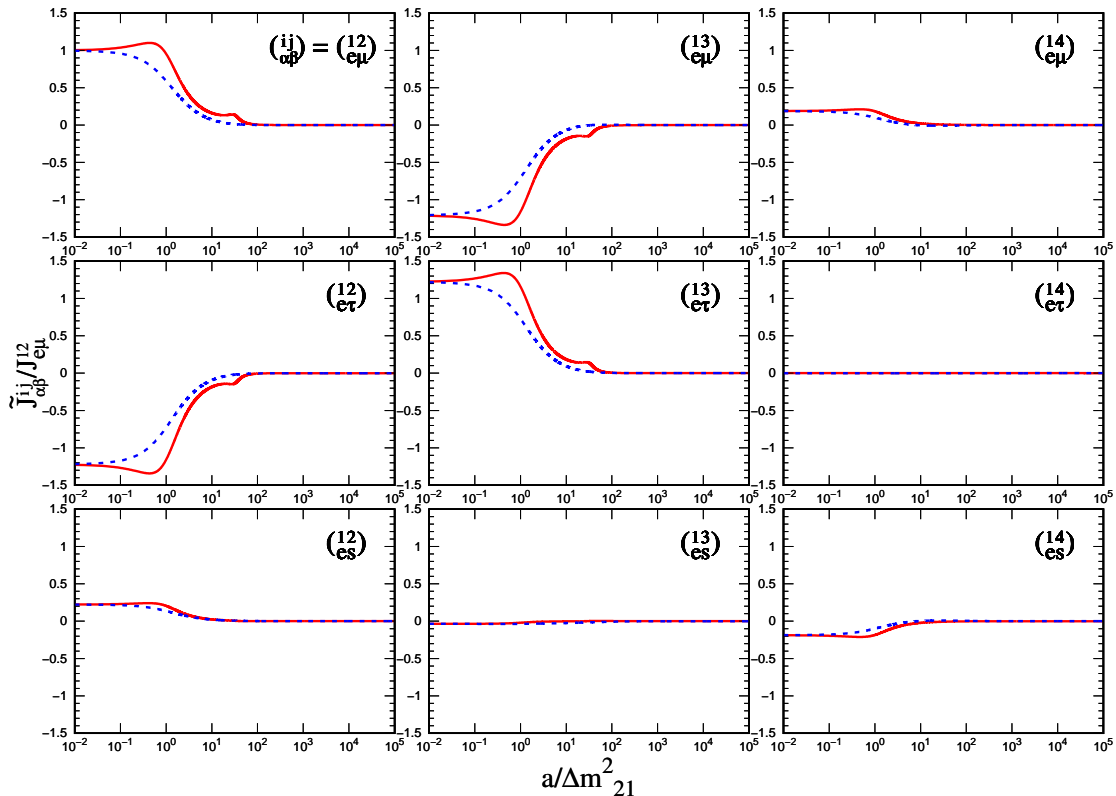


**Figure 2.** The evolution of the Jarlskog-like invariants  $\tilde{\mathcal{J}}_{\alpha\beta}^{ij}$  in NH case, normalized by  $\mathcal{J}_{e\mu}^{12}$ , with respect to  $a/\Delta m_{21}^2$ . The red solid and blue dashed curves correspond to the results of neutrino and antineutrino oscillations, respectively.

- While keeping the active-sterile mixings unchanged from the  $k = 0$  scenario of antineutrino case, two of the six mixing matrix elements of neutrino case ( $|V_{s1}|^2$  and  $|V_{s3}|^2$ ) change their behaviors.
- The value of  $|V_{s4}|^2$  is stably kept around one since the mixing among sterile neutrino and other ones is close to zero for the antineutrino case. The evolution for neutrino case differs as a sudden drop from unity to zero occurs around  $10^3$ , which is consistent with the behaviors of mixing among sterile neutrino and the active ones.

Similarly, the inverse mass hierarchy (IH) case as well as the evolution of effective masses, described in Eq. (2.7), can also be analyzed and we have neglected the corresponding plots. Now with the effective mixing matrix and mass square prepared, we may apply these results to further analyze neutrino propagation in typic mediums.

### 3.2 The evolution of Jarlskog-like invariants

For the nine Jarlskog-like invariants, the choice of the basis is not unique. Here we fix one of the flavor and mass indices as electron and 1 and let the remaining indices run over all the parameter space. In Fig. 2, within NH framework by setting  $k = 0$  we show

the evolution behaviors of these nine invariants normalized to the vacuum value of one invariant  $\mathcal{J}_{e\mu}^{12}$  with respect to  $a/\Delta m_{21}^2$ .

Typically the behavior of the Jarlskog-like invariant in the first plot of Fig. 2 can be interpreted from equation (2.14). Among all the terms in the right hand side, terms containing  $\Delta\tilde{m}_{21}^2$  dominate the evolution trend. During the initial stage, the increase of  $\tilde{\mathcal{J}}_{e\mu}^{12}$  is determined by positivity of  $(|V_{e1}|^2 - |V_{e2}|^2)\Delta\tilde{m}_{21}^2$ . At around  $a/\Delta m_{21}^2 \sim 1$ , the first resonance is approached for the sign flip of  $(|V_{e1}|^2 - |V_{e2}|^2)$ , see the first two plots in Fig. 1(a). And then a second peak appears at around  $a/\Delta m_{21}^2 \sim 10$ , due to the change of the relative size between  $|V_{e2}|^2$  and  $|V_{e3}|^2$ , which is consistent with the pure three-flavor situation. Analogically the other eight invariants can be analyzed and here we exhibit their evolutions as the remaining parts of Fig. 2, in which the sum rules in equation (2.13) are respected in each row or column.

### 3.3 The matter effects in Earth

Generally speaking, terrestrial matter effects should be taken into account in all the experiments taken place in Earth. Practically, there is few difference in the propagation between vacuum and matter in short-baseline (SBL) and medium-baselined (MBL) experiments. These experiments are usually built around sites nearby nuclear power plants with electron-type antineutrino as their source, given

$$P(\bar{\nu}_e \rightarrow \bar{\nu}_e) = \sum_i |V_{ei}|^4 + 2 \sum_{i<j} |V_{ei}|^2 |V_{ej}|^2 \cos \tilde{\Delta}_{ij}. \quad (3.1)$$

Since the matter effects are not significant, the mixing matrix and mass difference in above Eq. (3.1) can be safely replaced by the corresponding ones in vacuum.

To further study neutrino mass ordering and measure CP-violating phase in the mixing matrix, taking the neutrino produced from accelerators with high energy as the experiment source is a good choice. The more energetic neutrino is supposed to propagate in a longer distance and hence longer baselines are required as one of the experimental conditions. In the LBL experiments, the matter effects are no longer negligible. The baselines for two ongoing LBL experiments, NOvA (NuMI Off-axis electron Neutrino Appearance) and T2K (Tokai to Kamioka), are given as  $L = 810$  km and  $L = 295$  km, while the baseline is designed to be  $L = 1300$  km for the near-future Fermilab experiment DUNE (The Deep Underground Neutrino Experiment). In these LBL experiments with accelerator neutrino source, both flavor changing and conserving modes can be observed and more physical goals, such as the measurement of leptonic CP-violating phase, are supposed to be achieved. In presence of a light sterile neutrino, the number of CP-violating phases enhances to 3 and hence the reliance on phases is more complicated. To make use of previous numerical results of mixing matrix and mass square difference in RGE approach, the general expression for neutrino oscillation is preferred, giving

$$P(\nu_\mu \rightarrow \nu_e) = \sum_i |V_{\mu i}|^2 |V_{ei}|^2 + 2 \sum_{i<j} \left[ \text{Re}(V_{\mu i} V_{ej} V_{\mu j}^* V_{ei}^*) \cos \tilde{\Delta}_{ij} - \text{Im}(V_{\mu i} V_{ej} V_{\mu j}^* V_{ei}^*) \sin \tilde{\Delta}_{ij} \right]. \quad (3.2)$$

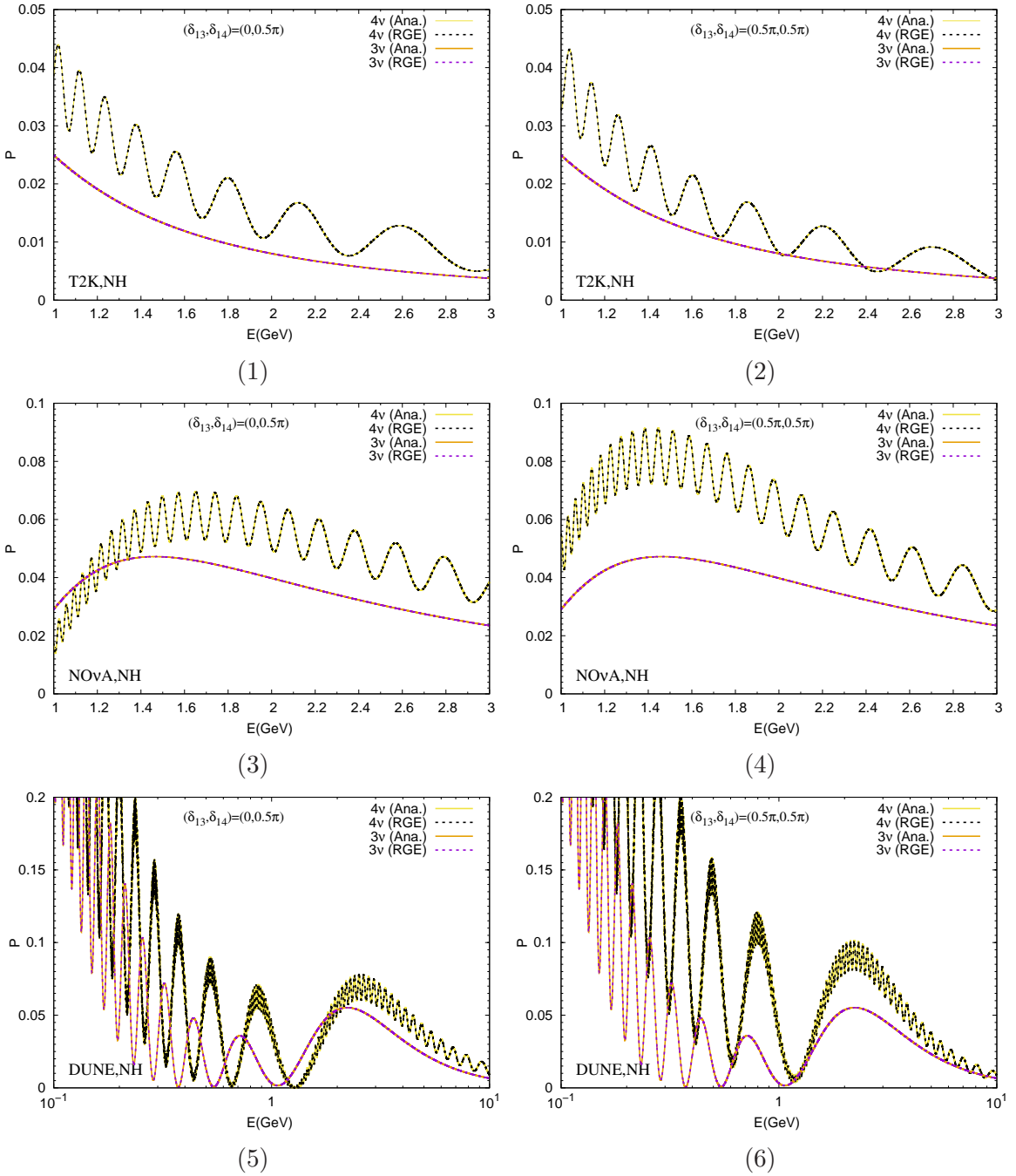


**Figure 3.** The oscillation probabilities of appearance mode  $\nu_\mu \rightarrow \nu_e$  in LBL accelerator neutrino experiments T2K, NOvA and DUNE for NH case with  $(\delta_{13}, \delta_{14}) = (0, \frac{\pi}{2}), (\frac{\pi}{2}, \frac{\pi}{2})$ .

For the three LBL experiments, though with different baselines, they share the common mixing matrix since the neutrinos received by detectors all travel through the crust. In the following analysis, we adopt the appearance mode as an illustration.

In the numerical calculations, the vacuum mixing (PMNS) matrix as well as particular mass-square differences are treated as the input. We adopt the values in [44] for three-flavor

situation and a global fit result [45] for the four-flavor case, summarized in Appendix A. To produce the curve  $P(E)$ , the  $E$  dependence of  $|V_{\alpha i}|^2$ ,  $V_{\alpha i}$  and  $\tilde{\Delta}_{ij}$  are required. These quantities are calculable by integrating related differential equations derived in Section 2.2.

In addition to plotting the oscillation curves of the three LBL experiments in RGE approach, we also make use of the exact analytical formulae derived in [27] to guarantee the effectiveness of this quantitative analysis based on RGE, shown in Fig. 3. We find that:

- All the curves plotted in two different ways coincide perfectly, indicating that the RGE approach works well in numerical study.
- The formulae developed in this work, including sterile neutrino contribution, can be utilized to describe four different situations ( $3\nu$  in vacuum and matter,  $4\nu$  in vacuum and matter) by opting for proper parameters.
- The matter effects are manifest for all the three LBL experiments. Although the orders of magnitude are of percentage level, with sterile neutrino the values of probability have a global enhancement. Taking NOvA with  $(\delta_{13}, \delta_{14}) = (0.5\pi, 0.5\pi)$  as an example (see Fig. 3(4)), the enhancement can reach as high as 100% when the energy of neutrino beam is around 1.5GeV. Obviously the future precise measurement from LBL accelerator neutrino experiments will provide complementary information of light sterile neutrino.

Now we have verified that the RGE approach is workable in quantitative study of neutrino oscillation in single constant density matter. We will explore the wider application with more complicated structure in the following part.

### 3.4 The day-night asymmetry of solar neutrino

Recently there have been some progresses in the study of solar neutrino. Neutrinos produced in the CNO fusion cycle have been observed [46], and the potential to observe  $^8\text{B}$  solar neutrino has been discussed [47]. In this part, we continue to study solar neutrino in the RGE approach as an extension of pure terrestrial matter effects.

Before being observed on the surface of earth during daytime, the electron-type neutrinos produced in solar core have travelled through solar matter, the vacuum between sun and earth, giving the  $\nu_e$  survival probabilities in the adiabatic approximation

$$P_D = \sum_{i=1}^4 P_{ei}^S P_{ie}^0, \quad (3.3)$$

where  $P_{ei}^S$  denotes the  $\nu_i$  component of  $\nu_e$  produced in solar core and its propagation to earth surface while  $P_{ie}^0$  stands for the probabilities of electron-type neutrino contained in the  $i$ -th mass eigenstate. The equation (3.3) is an extension of three-flavor framework [48], including the contribution from a light sterile neutrino contribution. Before arriving at the detectors on the other side of the incident point, solar neutrinos pass some distance inside



the earth at night and the extra earth matter effects should be taken into account. The nighttime  $\nu_e$  survival probability is then

$$P_N = \sum_{i=1}^4 P_{ei}^S P_{ie}^E, \quad (3.4)$$

where  $P_{ie}^E$  denotes the probability of  $\nu_i$  propagation in earth matter and finally captured by detector in  $\nu_e$  state. The day-night asymmetry stands for the probability difference between the day and night time, giving

$$\Delta P = P_D - P_N = \sum_{i=1}^4 P_{ei}^S (P_{ie}^0 - P_{ie}^E). \quad (3.5)$$

The calculation of  $\Delta P$  requires the information of  $P_{ei}^S$ ,  $P_{ie}^0$  and  $P_{ie}^E$ . In general, we have

$$P_{ie}^0 = |U_{ei}|^2, \quad P_{ei}^S = |V_{ei}^S|^2, \quad P_{ie}^E = |V_{ei}^E|^2 \quad (3.6)$$

with vacuum PMNS matrix  $U_{ei}$ , solar matter effective mixing matrix  $V_{ei}^S$  and earth matter effective mixing matrix  $V_{ei}^E$ . In the practical calculation, after producing in solar core<sup>3</sup>, we adopt adiabatic approximation to describe neutrino propagation through other part of the sun and the vacuum between sun and the Earth. For the Earth model, we take the slab approximation to describe the terrestrial matter[51]. Explicitly, the effective mixing matrix in Earth is in the form of

$$V^E = \left( \prod_{i=1}^N V_i e^{-iH_i L_i} V_i^\dagger \right) U, \quad (3.7)$$

where  $N$  is the number of slabs,  $H_i$  is the effective Hamiltonian after diagonalization in  $i$ -th layer with corresponding neutrino traveling distance  $L_i$  and effective mixing  $V_i$ . Here in 8-Layer Earth Model [51], including the structure of Inner Core, Outer Core, Mantel and Crust, the value of  $N$  depends on the zenith angle.

Although the mixing in Earth, equation (3.7), is complicated due to the multiple structures of the Earth, RGE approach provides a proper choice for realizing the calculation. Combining all the necessary mixings both in Earth and the sun, the electron-neutrino survival probabilities from solar neutrino in various conditions are numerically presented in Fig. 4. Some features can be drawn:

- In general, the survival probability in  $4\nu$  picture decreases compared with the corresponding one in  $3\nu$  picture. This is understandable as the sterile neutrino takes up part of the components of electron-neutrino produced in solar core, diminishing the survival probability.
- Though input parameter dependence exists, the difference is tiny between different parameter choices in  $4\nu$  framework.

---

<sup>3</sup>In solar core, taking  $N_e = 102N_A/\text{cm}^3$  for electron density [49] and  $N_n = 0.1639N_e$  for neutron density [50], we obtain the solar core matter parameter  $k = -0.5 \times 0.1639 \approx -0.08$ .

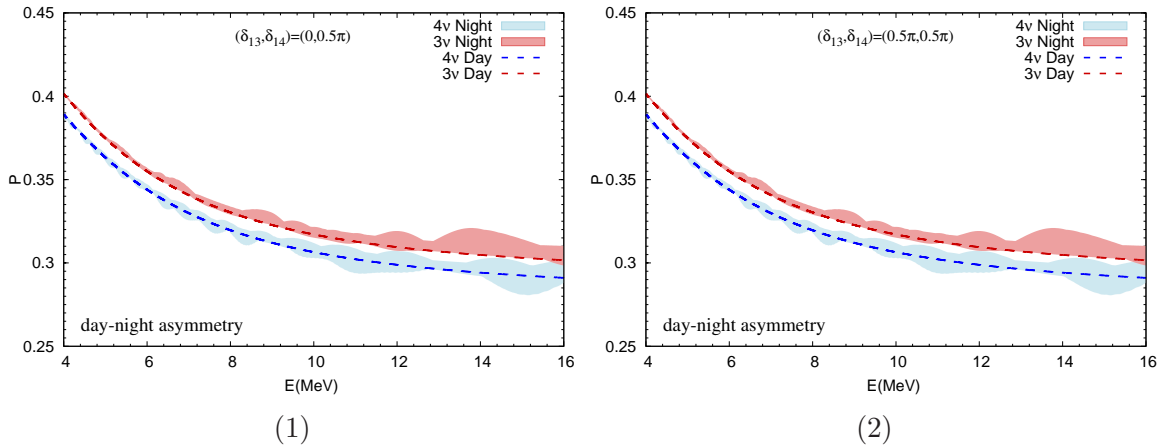


**Figure 4.** Electron-neutrino survival probabilities from solar neutrino in the three-flavor (red) and four-flavor (blue) pictures, in which the daytime behaviors are marked as dashed curves while nighttime ones vary in their corresponding colored ranges.

- The probability at nighttime, which depends on the altitude of incident beam, vary in a range due to the terrestrial matter effects.
- For the maxima of day-night asymmetry  $\Delta P$ , it can be reached around 13.5MeV for three-flavor case while 15MeV in the four-flavor framework. This could be further discriminated by future solar neutrino experiments.

As demonstrated in above quantitative analysis, the RGE approach to neutrino matter provides a proper tool in exploring objects with richer structures.

#### 4 Concluding remarks

The RGE has a wide application in many fields of modern physics. In the pioneering work, a connection between RGEs and neutrino matter effects in standard three-flavor picture has been established and a set of differential equations have been obtained[35]. To demonstrate the validity of RGE approach to matter effects in quantitative study is a worthy topic. Furthermore, to explore an extension of the entire methodology incorporating a light sterile neutrino is also valuable for the recent fast development of sterile neutrino-related experiments. These tasks have been achieved in current work.

In presence of a light sterile neutrino, we have derived a completed set of differential equations on effective mixing matrix elements, mass-square differences and Jarlskog-like invariants in RGE approach. By opting for proper input parameters (mixings and mass differences), these equations as well as their solutions can describe both three-flavor and four-flavor neutrino oscillation. The mixing parameters  $V_{\alpha i}$  and  $\tilde{m}_i^2$  depend on the matter parameter  $k$  in the constant density matter. Solving these differential equations, we carry out numerical analysis for the evolution of  $|V_{\alpha i}|^2$  and Jarlskog-like invariants. The consistence of three-flavor case with [35] is verified, which further guarantees the correctness

for further study. By combining three LBL neutrino experiments, we calculate their corresponding oscillation probabilities in NH scenario as examples of terrestrial matter effects. The study of electron-neutrino survival probabilities and hence day-night asymmetry of solar neutrino observed on the Earth surface is more complicated for types of mediums involved. Taking the adiabatic approximation for solar matter and slab approximation for terrestrial matter, we numerically calculate the survival probabilities at daytime and nighttime. The day-night asymmetry maximizes itself at around 13.5MeV in the standard three active flavor framework and 15MeV in four-flavor framework, which could be discriminated in future precise measurement.

The RGE approach developed in this work provides a complementary way to study neutrino phenomenology involving matter effects. On the other hand, the correctness of its application shown in this work helps us to have a deep understanding of RGE.

## Acknowledgments

We would like to thank Prof. Z.-z. Xing for his encouragement that produces the current work. Discussions with Prof. Jiajie Ling and Prof. Benda Xu are also acknowledged. This work is supported by NSFC under Grant No. U1932104 and No. 12142502, by Guangdong Provincial Key Laboratory of Nuclear Science with No. 2019B121203010.

## A Input parameters

Two types of input parameters, mixing matrix and masses in both three-flavor and four-flavor pictures, are summarize in Table 1.

**Table 1.** A summary of the involved input parameters in the numerical analysis of this work.

$\sin^2 \theta_{13}$	$\sin^2 \theta_{12}$	$\sin^2 \theta_{23}$	$\Delta m_{21}^2$	$\Delta m_{31}^2$	$\delta_{13}$
0.0220	0.307	0.546	$7.53 \times 10^{-5} \text{eV}^2$	$2.526 \times 10^{-3} \text{eV}^2$	$1.36\pi$
$\sin^2 \theta_{14}$	$\sin^2 \theta_{24}$	$\sin^2 \theta_{34}$	$\Delta m_{41}^2$	$\delta_{14}$	$\delta_{34}$
0.019	0.015	0	$0.1 \text{eV}^2$	$0.5\pi$	0

- Three-flavor framework

We adopt the standard parameterization of PMNS matrix and the inputs are taken from PDG [44].

- Four-flavor framework

We follow the convention in Appendix A of [27] to parameterize the four-dimensional mixing matrix with three leptonic CP-violating phases ( $\delta_{13}, \delta_{14}, \delta_{34}$ ). A global fit results [45] are taken as input here, in which  $\delta_{13}$  is kept as a free parameter.

## References

- [1] LSND collaboration, *Evidence for neutrino oscillations from the observation of  $\bar{\nu}_e$  appearance in a  $\bar{\nu}_\mu$  beam*, *Phys. Rev. D* **64** (2001) 112007 [[hep-ex/0104049](#)].
- [2] MINIBOONE collaboration, *Significant Excess of ElectronLike Events in the MiniBooNE Short-Baseline Neutrino Experiment*, *Phys. Rev. Lett.* **121** (2018) 221801 [[1805.12028](#)].
- [3] Y. Hino et al., *Characterization of the correlated background for a sterile neutrino search using the first dataset of the JSNS<sup>2</sup> experiment*, [2111.07482](#).
- [4] MICROBOONE collaboration, *Search for Neutrino-Induced Neutral Current  $\Delta$  Radiative Decay in MicroBooNE and a First Test of the MiniBooNE Low Energy Excess Under a Single-Photon Hypothesis*, [2110.00409](#).
- [5] MICROBOONE collaboration, *Search for an Excess of Electron Neutrino Interactions in MicroBooNE Using Multiple Final State Topologies*, [2110.14054](#).
- [6] C. A. Argüelles, I. Esteban, M. Hostert, K. J. Kelly, J. Kopp, P. A. N. Machado et al., *MicroBooNE and the  $\nu_e$  Interpretation of the MiniBooNE Low-Energy Excess*, [2111.10359](#).
- [7] P. Huber, *On the determination of anti-neutrino spectra from nuclear reactors*, *Phys. Rev. C* **84** (2011) 024617 [[1106.0687](#)].
- [8] G. Mention, M. Fechner, T. Lasserre, T. A. Mueller, D. Lhuillier, M. Cribier et al., *The Reactor Antineutrino Anomaly*, *Phys. Rev. D* **83** (2011) 073006 [[1101.2755](#)].
- [9] T. A. Mueller et al., *Improved Predictions of Reactor Antineutrino Spectra*, *Phys. Rev. C* **83** (2011) 054615 [[1101.2663](#)].
- [10] NEOS collaboration, *Sterile Neutrino Search at the NEOS Experiment*, *Phys. Rev. Lett.* **118** (2017) 121802 [[1610.05134](#)].
- [11] DANSS collaboration, *Recent results of the DANSS experiment*, *PoS EPS-HEP2019* (2020) 401 [[1911.10140](#)].
- [12] STEREO collaboration, *First antineutrino energy spectrum from  $^{235}\text{U}$  fissions with the STEREO detector at ILL*, *J. Phys. G* **48** (2021) 075107 [[2010.01876](#)].
- [13] A. P. Serebrov et al., *Search for sterile neutrinos with the Neutrino-4 experiment and measurement results*, *Phys. Rev. D* **104** (2021) 032003 [[2005.05301](#)].
- [14] PROSPECT collaboration, *Improved short-baseline neutrino oscillation search and energy spectrum measurement with the PROSPECT experiment at HFIR*, *Phys. Rev. D* **103** (2021) 032001 [[2006.11210](#)].
- [15] GALLEX collaboration, *Final results of the Cr-51 neutrino source experiments in GALLEX*, *Phys. Lett.* **B420** (1998) 114.
- [16] F. Kaether, W. Hampel, G. Heusser, J. Kiko and T. Kirsten, *Reanalysis of the GALLEX solar neutrino flux and source experiments*, *Phys. Lett.* **B685** (2010) 47 [[1001.2731](#)].
- [17] SAGE collaboration, *Measurement of the response of the Russian-American gallium experiment to neutrinos from a Cr-51 source*, *Phys. Rev.* **C59** (1999) 2246 [[hep-ph/9803418](#)].
- [18] J. N. Abdurashitov et al., *Measurement of the response of a Ga solar neutrino experiment to neutrinos from an Ar-37 source*, *Phys. Rev.* **C73** (2006) 045805 [[nucl-ex/0512041](#)].

- [19] T. Schwetz, *Status of sterile neutrino oscillations*, *Nucl. Phys. Proc. Suppl.* **235-236** (2013) 229.
- [20] J. Kostensalo, J. Suhonen, C. Giunti and P. C. Srivastava, *The gallium anomaly revisited*, *Phys. Lett.* **B795** (2019) 542 [[1906.10980](#)].
- [21] V. V. Barinov et al., *Results from the Baksan Experiment on Sterile Transitions (BEST)*, [2109.11482](#).
- [22] B. Dasgupta and J. Kopp, *Sterile Neutrinos*, *Phys. Rept.* **928** (2021) 63 [[2106.05913](#)].
- [23] M. S. Athar et al., *Status and Perspectives of Neutrino Physics*, [2111.07586](#).
- [24] L. Wolfenstein, *Neutrino Oscillations in Matter*, *Phys. Rev. D* **17** (1978) 2369.
- [25] S. P. Mikheev and A. Y. Smirnov, *Resonant amplification of neutrino oscillations in matter and solar neutrino spectroscopy*, *Nuovo Cim. C* **9** (1986) 17.
- [26] N. Klop and A. Palazzo, *Imprints of CP violation induced by sterile neutrinos in T2K data*, *Phys. Rev. D* **91** (2015) 073017 [[1412.7524](#)].
- [27] W. Li, J. Ling, F. Xu and B. Yue, *Matter Effect of Light Sterile Neutrino: An Exact Analytical Approach*, *JHEP* **10** (2018) 021 [[1808.03985](#)].
- [28] B. Yue, W. Li, J. Ling and F. Xu, *A compact analytical approximation for a light sterile neutrino oscillation in matter*, *Chin. Phys. C* **44** (2020) 103001 [[1906.03781](#)].
- [29] E. C. G. Stueckelberg de Breidenbach and A. Petermann, *Normalization of constants in the quanta theory*, *Helv. Phys. Acta* **26** (1953) 499.
- [30] M. Gell-Mann and F. E. Low, *Quantum electrodynamics at small distances*, *Phys. Rev.* **95** (1954) 1300.
- [31] K. G. Wilson, *Renormalization group and critical phenomena. 1. Renormalization group and the Kadanoff scaling picture*, *Phys. Rev. B* **4** (1971) 3174.
- [32] K. G. Wilson, *Renormalization group and critical phenomena. 2. Phase space cell analysis of critical behavior*, *Phys. Rev. B* **4** (1971) 3184.
- [33] S. H. Chiu, T. K. Kuo and L.-X. Liu, *Neutrino mixing in matter*, *Phys. Lett. B* **687** (2010) 184 [[1001.1469](#)].
- [34] S. H. Chiu and T. K. Kuo, *Features of Neutrino Mixing*, *Phys. Rev. D* **97** (2018) 055026 [[1712.08487](#)].
- [35] Z.-z. Xing, S. Zhou and Y.-L. Zhou, *Renormalization-Group Equations of Neutrino Masses and Flavor Mixing Parameters in Matter*, *JHEP* **05** (2018) 015 [[1802.00990](#)].
- [36] S. Zhou, *Continuous and discrete symmetries of renormalization group equations for neutrino oscillations in matter*, *J. Phys. G* **49** (2022) 025004 [[2004.10570](#)].
- [37] X. Wang and S. Zhou, *Analytical solutions to renormalization-group equations of effective neutrino masses and mixing parameters in matter*, *JHEP* **05** (2019) 035 [[1901.10882](#)].
- [38] C. Jarlskog, *Commutator of the Quark Mass Matrices in the Standard Electroweak Model and a Measure of Maximal CP Nonconservation*, *Phys. Rev. Lett.* **55** (1985) 1039.
- [39] W.-S. Hou, Y.-Y. Mao and C.-H. Shen, *Leading Effect of CP Violation with Four Generations*, *Phys. Rev. D* **82** (2010) 036005 [[1003.4361](#)].

- [40] Z.-z. Xing, *Sum rules of neutrino masses and CP violation in the four neutrino mixing scheme*, *Phys. Rev. D* **64** (2001) 033005 [[hep-ph/0102021](#)].
- [41] V. A. Naumov, *Three neutrino oscillations in matter, CP violation and topological phases*, *Int. J. Mod. Phys. D* **1** (1992) 379.
- [42] S. Toshev, *On T violation in matter neutrino oscillations*, *Mod. Phys. Lett. A* **6** (1991) 455.
- [43] F. Xu and S. Zeng, *work in progress*, .
- [44] PARTICLE DATA GROUP collaboration, *Review of Particle Physics*, *PTEP* **2020** (2020) 083C01.
- [45] S. Gariazzo, C. Giunti, M. Laveder and Y. F. Li, *Updated Global 3+1 Analysis of Short-BaseLine Neutrino Oscillations*, *JHEP* **06** (2017) 135 [[1703.00860](#)].
- [46] BOREXINO collaboration, *Experimental evidence of neutrinos produced in the CNO fusion cycle in the Sun*, *Nature* **587** (2020) 577 [[2006.15115](#)].
- [47] JUNO collaboration, *Feasibility and physics potential of detecting  $^8\text{B}$  solar neutrinos at JUNO*, *Chin. Phys. C* **45** (2021) 023004 [[2006.11760](#)].
- [48] E. K. Akhmedov, M. A. Tortola and J. W. F. Valle, *A Simple analytic three flavor description of the day night effect in the solar neutrino flux*, *JHEP* **05** (2004) 057 [[hep-ph/0404083](#)].
- [49] J. N. Bahcall, M. H. Pinsonneault and S. Basu, *Solar models: Current epoch and time dependences, neutrinos, and helioseismological properties*, *Astrophys. J.* **555** (2001) 990 [[astro-ph/0010346](#)].
- [50] M. Asplund, N. Grevesse, A. J. Sauval and P. Scott, *The chemical composition of the Sun*, *Ann. Rev. Astron. Astrophys.* **47** (2009) 481 [[0909.0948](#)].
- [51] A. M. Dziewonski and D. L. Anderson, *Preliminary reference earth model*, *Phys. Earth Planet. Interiors* **25** (1981) 297.